Monte Carlo Simulation of Partially Confined Flexible Polymers

G. F. Hermsen, B. A. de Geeter, N. F. A. van der Vegt,* and M. Wessling

Membrane Technology Group, Faculty of Chemical Technology, University of Twente, P.O. Box 217, 7500 AE Enschede, The Netherlands

Received February 4, 2002; Revised Manuscript Received April 18, 2002

ABSTRACT: We have studied conformational properties of flexible polymers partially confined to narrow pores of different size using configurational biased Monte Carlo simulations under athermal conditions. The asphericity of the chain has been studied as a function of its center of mass position along the pore axis and as a function of the degree of penetration, or fraction of confined segments. The asphericity passes through a maximum well before all segments are located inside the pore. Rather than deforming gradually, we find that at intermediate penetration degrees, where the center of mass is within distances of approximately one radius of gyration away from the pore entry, the chain part inside the pore stretches out considerably while the remaining part outside the pore is coillike ("flower conformations"). When the center of mass is located further inside the pore, this strong chain extension along the pore axis diminishes, and the average conformation becomes that of a deformed coil. Introduction of weakly attractive monomer−wall interactions does not affect these observations significantly.

Introduction

The shape of flexible polymers depends for a large extent on their environment, viz. polymer concentration, the presence of other components, solvent quality, and spatial confinements. Especially the shape of confined polymers and oligomers is a field of great interest, due to its significance in for example liquid chromatography, gel electrophoresis, oil recovery, and membrane-based separation processes.

Several computer simulation studies on confined polymers have been reported in the literature. Milchev et al.[1] performed simulations on polymer chains confined in straight tubes and compared their results with existing scaling arguments. Cifra and Bleha[2,3] used self-avoiding walk Monte Carlo simulations in a slitlike pore to find out the relation between the conformational behavior of confined chains and polymer concentration at Θ and athermal conditions. Varying the slit width, the coils adopted pancakelike conformations at small widths. Adsorption effects of polymer segments with the wall were not taken into account. The end-to-end distance became greater with smaller slit widths. Later studies also took attractive polymer−wall interactions[4] and chain flexibility[5] into account, and these findings confirm an analytical theory derived for a theoretical polymer chain between two repulsive plates by Shiokawa.[6,7] Also, the shape of small end-grafted polymer chains, for which scaling arguments do not really apply, was studied for various degrees of confinement.[8] Even the shape of confined polyelectrolytes has been studied.[9]

Some molecular dynamics studies take polymer−wall attractions into account: Zhang[10] studied linear decane films in carbon tubes with Lennard-Jones type segment−wall interactions and found that the chains aligned to the walls when close to the walls. Earlier, Boyd et al.[11] already studied effects of polymer shape of confined oligomers on partitioning. Aoyagi et al.[12] performed molecular simulations on melts of coarse-grained chains and found that polymers near the walls are deformed by attraction and the presence of other molecules and studied also the relaxation times of the chains in confinements for strong attractive segment−wall interactions. Brownian dynamics simulations of hydrocarbons in (biological) membranes were carried out to cover greater time intervals.[13] These studies were all for fully confined polymers.

Escape transitions of end-grafted polymer chains from a confinement of two opposing walls of a piston are found[14,15] for various chain lengths. When varying the width of the confinement between the walls, they found a relation for the escape width as a function of polymer length and piston radius. These polymers burst out at a certain width whereafter the radius of gyration increases considerably. This transition is sharper for increasing chain lengths. A study of polymers confined inside a sphere escaping through a small hole to a bulk phase has also been done.[16−18] Here a free energy barrier is found in the transition from confinement to bulk.

Conformations of end-grafted polymers have been studied close to an interface modeled by a stepwise external potential. The authors found a transition of a coillike to a flowerlike conformation: a stretched stem of segments and, in the region of lower monomer potential, a coillike crown containing the remaining segments.[19,20] Such flower conformations are very similar to the conformations found in this article for very small pores.

Although a lot is known about conformational behavior of confined polymers, the intermediate conformations adopted by a polymer entering a pore from the bulk solution is still a rather unexplored yet important field. For example, entropic trapping of DNA molecules in microsized (wide) regions separated by nanofluidic (narrow) channels (smaller than the DNA radius of gyration) has been reported as a mean to separate long DNA molecules[21,22] in a practically integrated DNA analysis system. The trapped DNA molecules escape with a probability which is determined by the ease at which a small part of the DNA molecule can enter the narrow channel.

In this article we show that chain conformations of partially confined flexible polymers are very much

* Corresponding author: e-mail n.f.a.vandervegt@ct.utwente.nl.

10.1021/ma020176g CCC: $22.00
Published on Web 05/24/2002

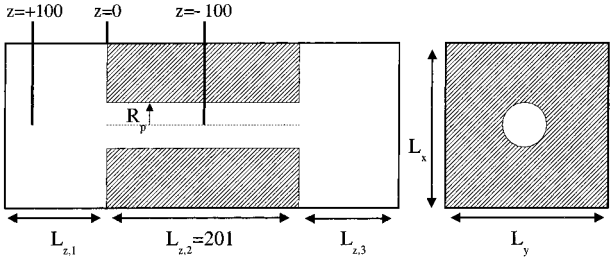

Figure 1. Geometrical details of the simulation box.

different from the ones adopted at full confinement. It is the purpose of this article to find out how a polymer conformation exactly changes at different degrees of penetration in cylindrical pores of various size. Monte Carlo simulations are used to sample the conformational space of a flexible polymer model under good solvent conditions.

Simulation Details

A discrete configurational bias Monte Carlo (CBMC)[23] method is used to carry out the simulations, combined with the bond fluctuation method[24] to model the polymers. All simulated polymers are 50 monomers (M) long, each monomer taking up eight gridpoints (a box) on a 3D simulation grid. Apart from their excluded-volume interactions, no additional thermal interactions between monomers are taken into account; hence, the simulations are performed under good solvent conditions. The interaction of one polymer segment with the (pore) wall is the summed interaction potential of the four gridpoints that are in direct contact with the wall and equals in total $0.0kT$ (no attraction) and $0.8kT$ (weak attraction). Note that $T = 0.92$ is the critical adsorption point of our model.[25]

Because the bond-fluctuation model allows for the CBMC algorithm to let each segment explore 108 directions—making it effectively an off-lattice case—the procedure is very time-consuming. For this reason all conformations are grown by choosing each new monomer growth direction from a set of 50 directions randomly selected from the complete list of 108 possibilities. The bias introduced using the CBMC method is removed in the acceptance rule

$$\mathrm{acc(o\rightarrow n)} = \min\left(1, \frac{W(\mathrm{n})}{W(\mathrm{o})}\right) \qquad (1)$$

in which W(n) and W(o) are the Rosenbluth factors of the new and old conformation, respectively.[23]

The simulation box is set up by putting a wall with a single straight pore in the middle of the box. The length of the cylindrical pore is large enough for the polymer to stretch completely without finding both ends at opposite pore mouths (Figure 1). The radius of the pore is based on the radius of gyration, R_g, of the polymer under athermal conditions in the bulk solution, where the R_g is 11.3 gridpoints big. The dimensions of the simulation box are $L_{z,1} = L_{z,3} = 90$ gridpoints, $L_{z,2} = 201$ gridpoints, and $L_x = L_y = 82$ gridpoints. The MC simulations are performed as follows: we start the MC algorithm on the pore axis by placing the first monomer at a fixed value of z ($z = -100$) and next grow the chain to obtain an initial chain conformation. A total of 20 000 chain growth attempts are next performed all starting with the same z-position of the first monomer accepting each new conformation according to eq 1. Averages are updated each four MC steps. Next we repeat this procedure by incrementing z by +1 lattice spacing until $z = 100$ has been reached. The conformations grown at $z = +100$ do not experience the wall and resemble unconfined polymers in a good solvent. The conformations grown at $z = -100$ are fully confined by the pore geometry. The pore radius R_p is varied such that $\lambda = R_g/R_p$ varies between $\lambda = 1.6$ and $\lambda = 0.5$.

Accompanied with conformational changes, the increase of the (excess) free energy of a chain as a function of its center of mass position (along the pore axis) may serve to define the transition region between bulk solution and bulk confinement. This quantity may be obtained from the probability to successfully insert a particle in the system, which in the Rosenbluth sampling scheme equates to the average Rosenbluth factor $\langle W\rangle$ obtained by averaging over all growth attempts. The excess free energy is obtained from $\beta F_{ex} = -\ln\langle W\rangle$.[23]

We calculated the free energy as a function of the chain center of mass position along the pore axis from $z = -100$ to $z = +100$. At each position of z we performed 20 000 growth attempts by placing the first monomer at this particular value of z and next growing the entire chain. Subsequently, we computed the z-component of the center of mass position of each generated conformation and updated a histogram at the appropriate entry (the bin value representing the center of mass z-component) with the chain Rosenbluth factor W.

The center of mass of incomplete chains resulting from failed growth attempts (where a term $W = 0$ is contributing to the average Rosenbluth factor) was calculated using only the successfully grown monomers in the chain. In a case of unsuccessfull growth, the growth usually breaks off between the 30th and the last monomer so the calculated center of mass for incomplete polymer chains will be close to a fully grown chain. Around 10% of the growth attempts in small confinements ($\lambda = 1.6$) is unsuccessful. Almost all growth attempts in the bulk are successful.

All simulations are carried out on Compaq Alphastation XP1000 workstations and Silicon Graphics Origin 200 workstations. The graphical snapshots are generated with gOpenMol 1.4.[26]

Results

Conformational Changes and Conformation Free Energy of Partly Confined Polymers. Figure 2 shows a series of snapshots of chain conformations with different degrees of penetration ϕ, which is equivalent to the fraction of confined segments of the polymer chain ($\lambda = 1.6$). In the bulk solution (A) and the bulk part of the pore (E) the chain assumes a coiled conformation. At intermediate degrees of penetration (B–D) the chain conformations look different: the part of the chain being confined stretches out considerably, while the remainder of the chain just outside the pore forms a relatively dense coil. This observation is reminiscent of the coil-to-flower transition observed for polymers pinned near a stepwise external potential.[19,20] The flower conformation features a strongly stretched stem from the grafting point to the interface and, on top of it, a crown composed of the remaining chain segments. If the grafting point is located far enough inside the pore, the increasing number of segments contributing to the stem will cause the conformational entropy to reduce below that of a fully confined (deformed) coil. Hence, a transition from

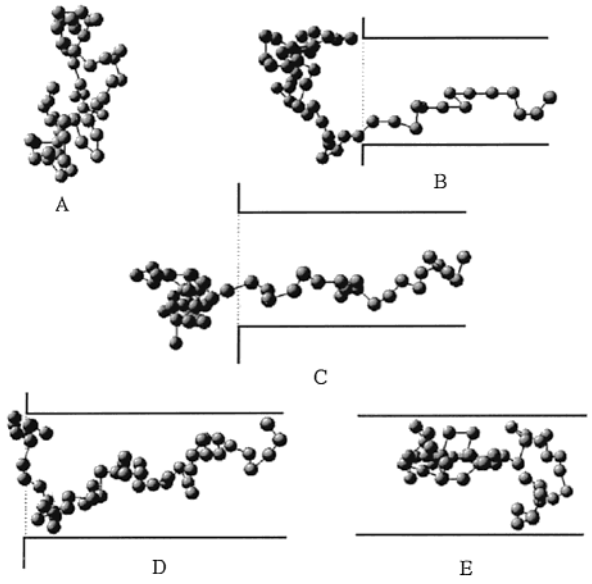

Figure 2. Snapshots of various degrees of polymer penetration ϕ: (A) bulk, (B) $\phi = 28\%$, (C) $\phi = 42\%$, (D) $\phi = 89\%$, and (E) bulk pore.

flowers to deformed coils occurs at some point. (We will show below that this transition occurs if the center of mass position of the chain exceeds beyond approximately $2R_g$ inside the pore.)

Figure 3 shows the conformational excess free energy along the axial pore direction as a function of the chain center of mass position. Figure 3A shows the free energy in case there are no attractive monomer−wall interactions, while in Figure 3B a weak interaction of $0.8kT$ was applied. This weak attraction lowers the free energy substantially, whereas it affects the strong conformational transition discussed above only a little (see below). Starting from the bulk solution in Figure 3A, the free energy starts to increase at distances of approximately 18 grid points (about 1.6 times the radius of gyration of the polymer chain in solution) away from the interfaces with pore dimensions $\lambda = 1.0$ and 1.6. For $\lambda = 0.5$ the increase starts at a slightly smaller distance. The free energy profile turns from convex into concave just in front of the pore entry, which is likely due to the fact that at this close proximity parts of the chain enter the pore. The free energy increases monotonically until it reaches a constant value at approximately $z = -10$ ($\lambda = 0.5$), $z = -15$ ($\lambda = 1.0$), and $z = -20$ ($\lambda = 1.6$). The extension of the transition region between the two values of constant free energy increases with the value of λ.

If a weak monomer−wall interaction of $0.8kT$ is introduced (Figure 3B), the extension of the transition region reduces. Starting from the bulk solution, the free energy profiles start to rise only at a distance of about 10 gridpoints away from the surface. Apparently here, the energy gained in the event of monomer adsorption onto the wall avoids the free energy from incrementing up to this small distance. The free energy reaches a constant value inside the pore at distances slightly closer to the interface for all three values of λ presented here.

Chain Asphericity. To quantify conformational change as a function of pore penetration, one may determine the change of the radius of gyration parallel $\langle R_{g\parallel}^2 \rangle$ and perpendicular $\langle R_{g\perp}^2 \rangle$ to the pore axis as a function of the penetration degree ϕ inside the pore.

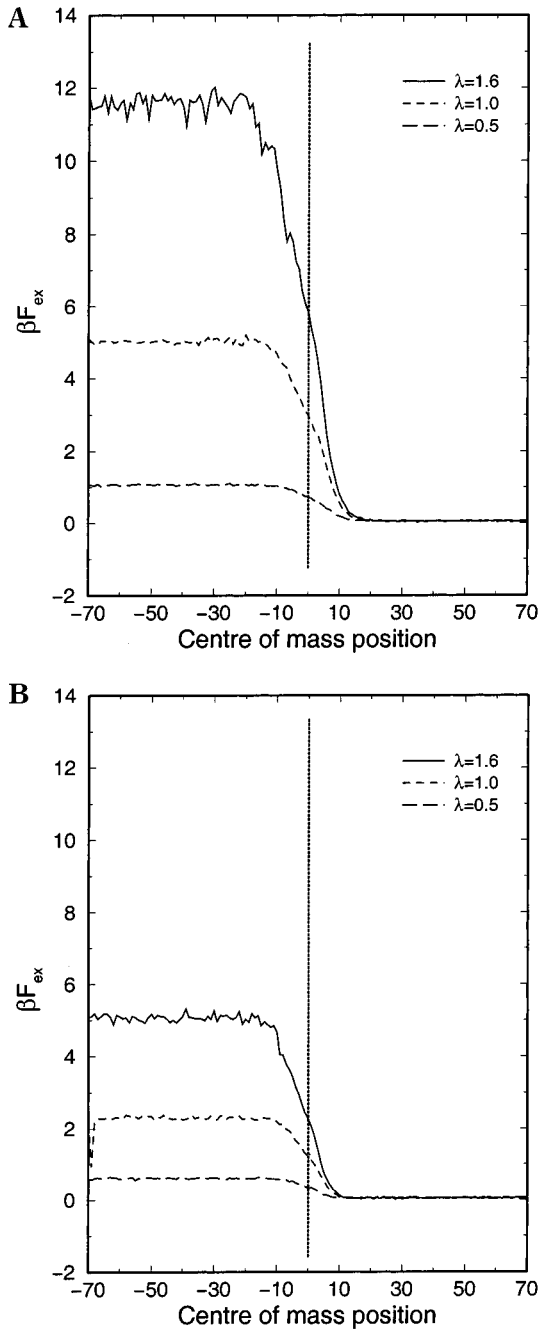

Figure 3. Free energy of the average polymer conformation as a function of the position of the polymer center of mass for $\lambda = 1.6$, 1.0, and 0.5 and different monomer−wall interactions: (A) $\epsilon_{pw} = 0kT$ and (B) $\epsilon_{pw} = 0.8kT$.

Figure 4A shows this for $\epsilon_{pw} = 0.0kT$ for $\lambda = 1.6$ and 1.0. An increasing ϕ results in a rise in $\langle R_{g\parallel}^2 \rangle$ until a maximum is reached at around 75%. At this point $\langle R_{g\parallel}^2 \rangle$ has increased from 43 to a value of 200 and from 43 to 125 for $\lambda = 1.6$ and $\lambda = 1.0$, respectively. Increasing the penetration degree to $\phi = 100\%$ results in a drop of $\langle R_{g\parallel}^2 \rangle$ to 125 and 75 for $\lambda = 1.6$ and 1.0, respectively. At the same time the $\langle R_{g\perp}^2 \rangle$ decreases from a free chain value 43 at $\phi = 0\%$ to the respective values around 7 and 13 at $\phi = 100\%$ for $\lambda = 1.6$ and 1.0. A greater λ value thus results in a stronger extension of the polymer in the direction of the pore axis for larger percentages of ϕ and a stronger contraction in the directions perpendicular to the pore axis. Figure 4B shows the results for $\epsilon_{pw} = 0.8kT$. Similar effects can be observed here,

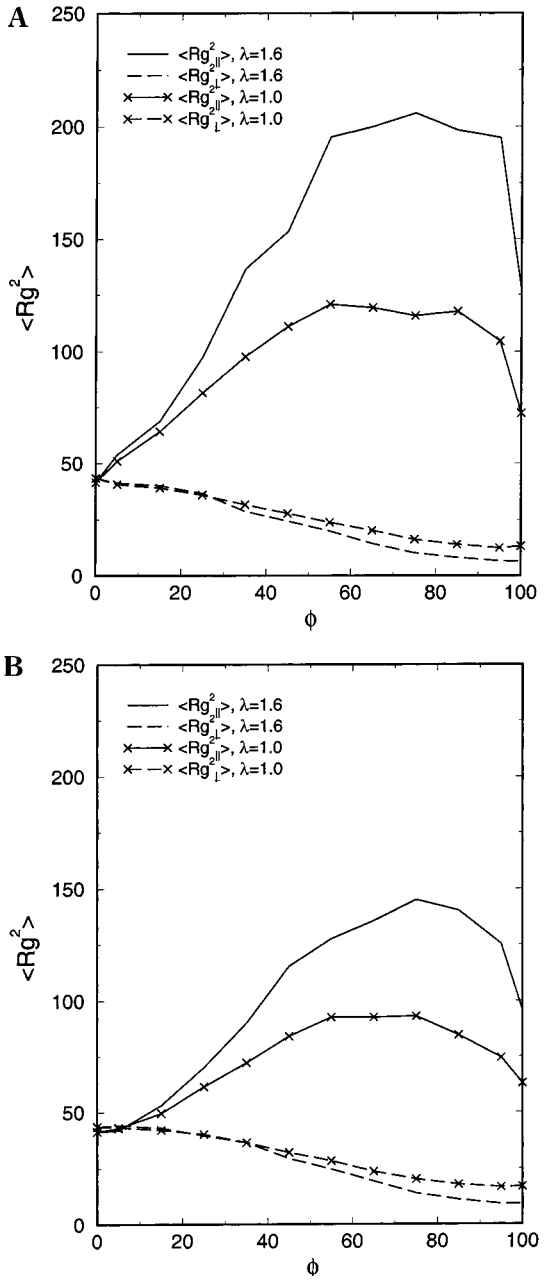

Figure 4. $\langle R^2_{g\parallel}\rangle$ and $\langle R^2_{g\perp}\rangle$ for $\lambda = 1.6$ and $\lambda = 1.0$ at monomer−wall interactions ϵ_{pw} of (A) $0.0kT$ and (B) $0.8kT$.

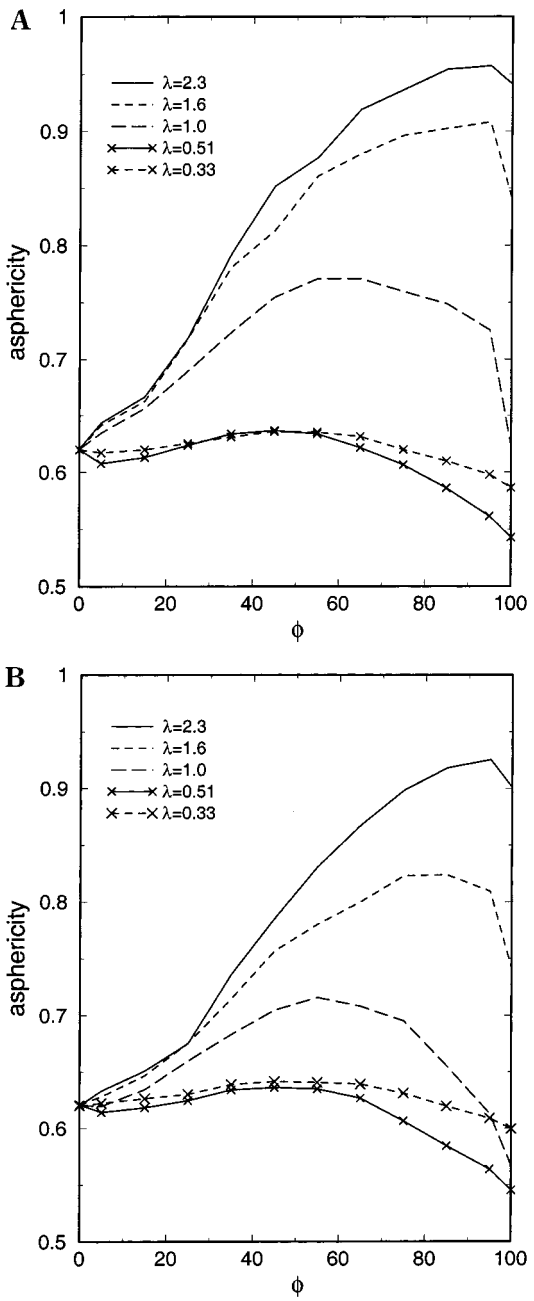

Figure 5. Asphericities of partially confined polymers at (A) $\epsilon_{pw} = 0kT$ and (B) $\epsilon_{pw} = 0.8kT$.

but the deformation in both directions is less strong: the maximum value of $\langle R^2_{g\parallel}\rangle$ for $\lambda = 1.6$ is 150 instead of 200 for $\epsilon_{pw} = 0.0kT$ and ends at 100 instead of 125. Also, the $\langle R^2_{g\perp}\rangle$ decays slower and levels off to a higher value than for $\epsilon_{pw} = 0.0kT$.

To account for the chain deformation in a single quantity, we invoke the "chain asphericity" in the remainder of this paper. The asphericity is obtained from the radius of gyration tensor $S_{ij} = (1/50)\sum_{n=1}^{50}(r_{n,i} - r_i^{cm})(r_{n,j} - r_j^{cm})$, which is calculated for each generated chain conformation and next diagonalized. The three eigenvalues obtained by this procedure provide information about the average shape of the polymer. We use these eigenvalues to define the asphericity A of the coil:[27]

$$A = 0.5\left(\frac{3V_1}{V_1 + V_2 + V_3} - 1\right) \qquad (2)$$

where V_1 is the largest eigenvalue and V_3 is the smallest eigenvalue of matrix S. The asphericity A equals 0 when the polymer coil takes on the shape of a perfect sphere. An infinitely thin cylinder has an asphericity $A = 1$. In bulk (athermal) solution the polymer studied (chain length 50) has an asphericity $A_{bulk} = 0.61$.

Figure 5 presents the asphericity for $\epsilon_{pw} = 0.0kT$ obtained with various pore sizes as a function of degree of penetration ϕ. For $\lambda \leq 1.0$ (large pores), A increases up to $\phi \approx 50\%$ and next decreases again. For $\lambda = 0.51$ and $\lambda = 0.33$ the increase of A is very moderate; noteworthy, at $\phi = 100\%$, it decreases below its value in bulk solution. This effect becomes less for the smaller λ values. When $\lambda > 1.0$ (small pores), the asphericity keeps on increasing until $\phi \approx 95\%$ has been reached, whereafter it makes a steep drop at 100% confinement. This drop is caused by the sudden flower-to-coil transition shown in Figure 2D,E. For $\lambda = 2.3$, the asphericity

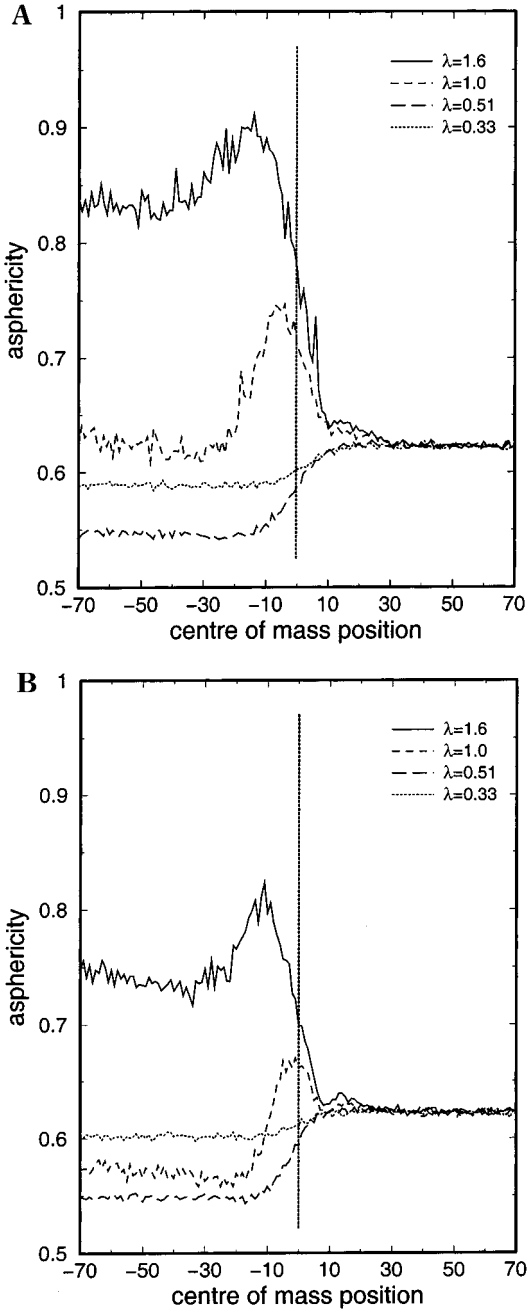

Figure 6. Asphericity vs center of mass position for $\lambda = 1.6$, 1.0, and 0.5 at (A) $\epsilon_{pw} = 0kT$ and (B) $\epsilon_{pw} = 0.8kT$.

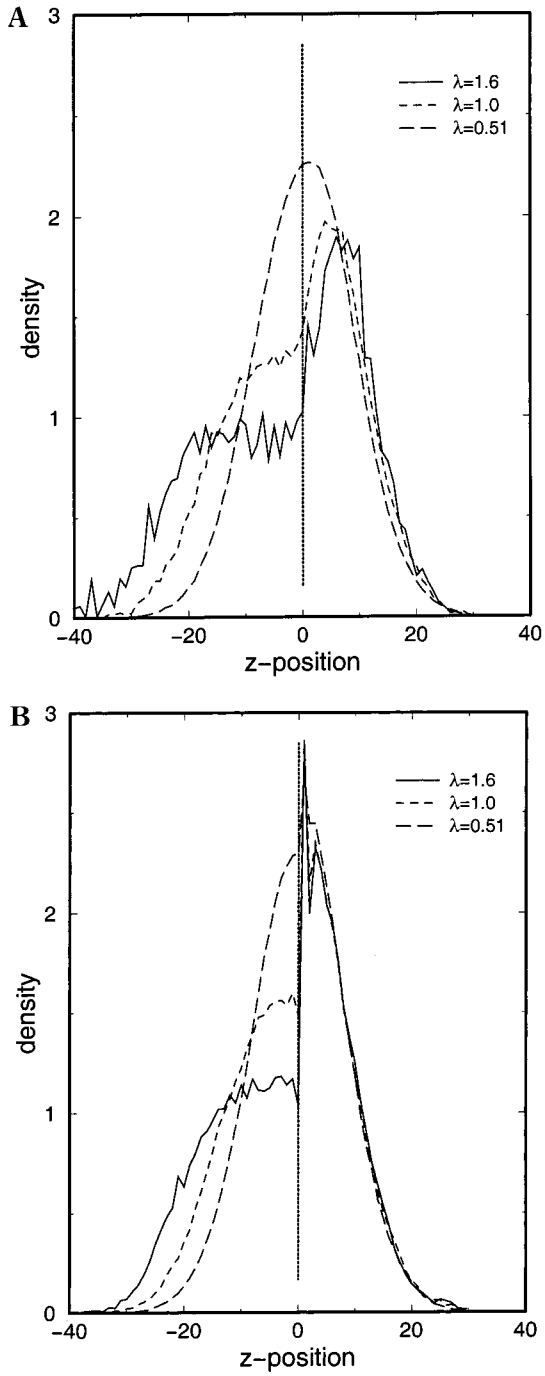

Figure 7. Monomer density vs center of mass position when $\phi = 50\%$ for $\lambda = 1.6$, 1.0, and 0.5 at (A) $\epsilon_{pw} = 0kT$ and (B) $\epsilon_{pw} = 0.8kT$.

raises above 0.95, indicating that with this small pore radius the chain almost fully extends one-dimensionally. Figure 5B shows the asphericities for the same λ values but now with an attractive monomer−wall interaction $\epsilon_{pw} = 0.8kT$. The effects observed above with $\epsilon_{pw} = 0.0kT$ are seen here as well; however, the asphericities tend to be somewhat smaller ($\lambda \geq 1.0$). This follows our intuition, since the entropy-driven conformational transition in Figure 2, during which the chain tends to keep as many monomers as possible outside the pore, now competes with energetically favorable monomer adsorption phenomena, which may occur at any point on the pore wall. With the weak adsorption energy used here flower conformations at intermediate degrees of penetration still dominate the average conformational properties.

Parts A and B of Figure 6 show the chain asphericities as a function of the chain center of mass position along the pore axis for $\epsilon_{pw} = 0.0kT$ and $\epsilon_{pw} = 0.8kT$, respectively. The dashed vertical line at $z = 0$ shows the location of the interface. For $\lambda = 1.6$, the asphericity starts to increase before the chain center of mass has entered the pore and reaches a maximum at approximately $z = -12$ after which it reduces to a constant value. With a pore size $\lambda = 1.0$, this maximum shifts closer to the interface. With $\lambda = 0.51$ and $\lambda = 0.33$ no maximum occurs, and the asphericity starts to drop from its value in the bulk solution just in front of the pore and levels off to a smaller value inside the pore (Figure 6A). These smaller values of A are probably caused by the fact that a certain number of chain conformations that run into the direction of the pore wall are reflected once they approach it, rendering the

average conformation somewhat more spherical compared to the conformation in the bulk solution. This effect is strongest with $\lambda = 0.51$ (Figure 6A) and diminishes again if the pore radius is made even bigger ($\lambda = 0.33$). The conformational properties of completely confined chains is discussed in more detail in ref 28. With $\lambda = 1.0$ and, more obvious, $\lambda = 1.6$ a much stronger confinement causes the monomer units to preferentially succeed along the pore axis (see Figure 7), and the asphericity never drops below the value in bulk solution. Noteworthy, if a weak monomer−wall interaction is introduced (Figure 6B), the situation changes; in this case the curve for $\lambda = 1.0$ drops below that of $\lambda = 0.33$ once the chain center of mass position proceeds beyond $z = -10$ to smaller z values. This effect is likely caused by a competition between confinement, which promotes extension of the chain in the z-direction, and adsorption effects, which promote extension in the directions perpendicular to the z-axis.

Monomer Density Profiles along the Pore Axis. Figure 7A,B shows the monomer density profiles along the z-direction for three values of λ. The curves apply to those conformations that have $\phi = 50\%$ of their segments confined. Again, a dashed vertical line at $z = 0$ emphasizes the location of the interface. In the absence of monomer−wall attraction (Figure 7A), the monomer density profile for $\lambda = 0.51$ follows a Gaussian distribution, indicating that this pore is big enough to not significantly affect the distribution of monomers inside the coil. With $\lambda = 1.0$ a maximum appears just outside the pore, and a plateau value occurs just inside. These figures signify the "crown" and "stem" parts of the flower conformation that appears at this pore size. If λ increases to 1.6, the plateau value drops below 1 monomer per lattice position and extends to regions further inside the pore. The magnitude of the maximum just outside the pore does not significantly change. Figure 7B shows the density profiles for the same values of λ, but now with a weak monomer−wall attraction of $0.8kT$. Clearly, at the bulk solution side of the interface, strong adsorption peaks can be identified. Inside the pore ($\lambda = 1.0$ and $\lambda = 1.6$), the density plateaus are still present but extend less far, which indicates that the extension of the stem gets smaller due to monomer adsorption onto the pore wall.

Summary and Conclusions

Configurational bias Monte Carlo (CBMC) simulations together with the bond fluctuation model have been used to study the confinement free energy and conformational properties of athermal flexible polymers partially confined to cylindrical pores with variable diameters. Simulations were performed without attractive monomer−wall interactions as well as with a weak interaction of $0.8kT$ per segment. For small pores ($\lambda \equiv R_g/R_{pore} \geq 1.0$, with R_g denoting the chain radius of gyration in bulk solution) the chain adopts a flower-type conformation characterized by a strongly stretched "stem" inside the pore and on top of it, just outside the pore, a "crown" composed of the remaining segments. The conformation turns into a (deformed) coil as soon as the chain center of mass position extends as far as approximately $2R_g$ inside the pore. Monomer adsorption onto the pore wall and the outer surface (facing the bulk solution) interferes with this picture to some extent. It causes the stem to become less extended and the crown to adsorb onto the surface.

Several properties, such as solvent quality, chain length, and chain flexibility, have not been considered in this work yet are likely to affect the conformational changes. These properties will be subject to future studies.

References and Notes

(1) Milchev, A.; Paul, W.; Binder, K. *Macromol. Theory Simul.* **1994**, *3*, 305−323.
(2) Cifra, P.; Bleha, T. *Macromol. Theory Simul.* **1999**, *8*, 603−610.
(3) Cifra, P.; Bleha, T. *Macromol. Theory Simul.* **2000**, *9*, 555−563.
(4) Cifra, P.; Bleha, T. *Polymer* **2000**, *41*, 1003−1009.
(5) Cifra, P.; Bleha, T. *Macromolecules* **2001**, *34*, 605−613.
(6) Shiokawa, K. *Polym. J.* **1990**, *22*, 925−935.
(7) Shiokawa, K. *Polym. J.* **1991**, *23*, 885−893.
(8) Arteca, G. A.; Edvinsson, T.; Elvingson, C. *Phys. Chem. Chem. Phys.* **2001**, *3*, 3737−3741.
(9) Park, P. J.; Chun, M.; Kim, J. *Macromolecules* **2000**, *33*, 8850−8857.
(10) Zhang, F. *J. Chem. Phys.* **1999**, *111*, 9082−9085.
(11) Boyd, R. H.; Chance, R. R.; Ver Strate, G. *Macromolecules* **1996**, *29*, 1182−1190.
(12) Aoyagi, T.; Takimoto, J.; Doi, M. *J. Chem. Phys.* **2001**, *115*, 552−559.
(13) Fernandes, M. X.; Huertas, M. L.; Castanho, M. A. R. B.; Garcia de la Torre, J. *Biochim. Biophys. Acta* **2000**, *1463*, 131−141.
(14) Milchev, A.; Yamakov, V.; Binder, K. *Phys. Chem. Chem. Phys.* **1999**, *1*, 2083−2091 and references therein.
(15) Milchev, A.; Yamakov, V.; Binder, K. *Europhys. Lett.* **1999**, *47*, 675−680.
(16) Sung, W.; Park, P. J. *Phys. Rev. Lett.* **1996**, *77*, 783−786.
(17) Park, P. J.; Sung, W. *Phys. Rev. E* **1998**, *57*, 730−734.
(18) Muthukumar, M. *Phys. Rev. Lett.* **2001**, *86*, 3188−3191.
(19) Skvortsov, A. M.; Klushin, L. I.; van Male, J.; Leermakers, F. A. M. *J. Chem. Phys.* **2001**, *115*, 1586−1595.
(20) Leermakers, F. A. M.; van Male, J.; Skvortsov, A. M. *Macromolecules* **2001**, *34*, 8294−8302.
(21) Han, J.; Turner, S. W.; Craighead, H. G. *Phys. Rev. Lett.* **1999**, *83*, 1688−1691.
(22) Han, J.; Craighead, H. G. *Science* **2000**, *288*, 1026−1029.
(23) Frenkel, D.; Smit, B. *Understanding Molecular Simulation: From Algorithms to Applications*, 2nd ed.; Academic Press: New York, 2002.
(24) Carmesin, I.; Kremer, K. *Macromolecules* **1988**, *21*, 2819−2823.
(25) Lai, P.K. *Phys. Rev. E* **1994**, *49*, 5420−5430.
(26) http://www.csc.fi/ laaksone/gopenmol/gopenmol.html.
(27) Schmitz, H.; Muller-Plathe, F. *J. Chem. Phys.* **2000**, *112*, 1040−1045.
(28) van Vliet, J. H.; Luyten, M. C.; ten Brinke, G. *Macromolecules* **1992**, *25*, 3802−3806.

MA020176G